



OPEN

Emission characteristics variation of GaAs_{0.92}Sb_{0.08}/Al_{0.3}Ga_{0.7}As strained multiple quantum wells caused by rapid thermal annealing

Dengkui Wang¹, Xian Gao^{1,2}, Jilong Tang^{1✉}, Xuan Fang¹, Dan Fang¹, Xinwei Wang¹, Fengyuan Lin¹, Xiaohua Wang¹, Rui Chen² & Zhipeng Wei^{1✉}

Rapid thermal annealing is an effective way to improve the optical properties of semiconductor materials and devices. In this paper, the emission characteristics of GaAs_{0.92}Sb_{0.08}/Al_{0.3}Ga_{0.7}As multiple quantum wells, which investigated by temperature-dependent photoluminescence, are adjusted through strain and interfacial diffusion via rapid thermal annealing. The light-hole (LH) exciton emission and the heavy-hole (HH) exciton emission are observed at room temperature. After annealing, the LH and HH emission peaks have blue shift. It can be ascribed to the variation of interfacial strain at low annealing temperature and the interfacial diffusion between barrier layer and well layer at high annealing temperature. This work is of great significance for emission adjustment of strained multiple quantum wells.

GaAsSb alloy is one of the potential candidates for infrared optoelectronics due to its large lattice bowing parameter and tunable band gap^{1,2}. Meanwhile, the multiple quantum wells (MQWs) possess higher emission efficiency than semiconductor films³. GaAsSb-based MQWs have been recognized as the important structures for fabricating infrared semiconductor laser. Up to now, great deals of III-V MQWs have been thoroughly investigated, such as GaAs/AlGaAs MQWs⁴, InGaAs/GaAs MQWs⁵, and InGaAs/GaAsP MQWs⁶. Moreover, the strain has great advantage of low threshold current density and high emission efficiency for MQWs laser⁷. It plays an important role in adjusting the optical characteristics of semiconductor laser. Hence, revealing the relationship of optical properties and strain is great significance for application of GaAsSb-based strained MQWs.

Generally speaking, rapid thermal annealing (RTA) is an effective way to enhance the optical properties of semiconductor materials through improving the composition homogeneity and decreasing the non-radiative defects concentration, which are introduced by asymmetry fluctuation of alloy components and intrinsic defects^{8–12}. However, the significant effect factors on optical properties of strained MQWs are not only material intrinsic defects but also device structural imperfect, such as, residual strain and interface^{13,14}. The residual strain, which sensitive to annealing temperature, is crucial importance for the emission characteristics of strained MQWs¹⁵. For example, tensile strain in well layers causes the valence band to move up and compressive strain in well layers cause valence band to moves down. Furthermore, the strains in MQWs lead to the splitting of heavy holes (HH) band with light holes (LH) band¹⁶. On the other hand, interfacial diffusion is also inevitable during annealing process. The diffusion between barrier layer and well layer leads to band bending and broadening¹⁷. So, the influence of RTA on strained MQWs is complex and need to further study.

In this paper, a kind of type-I GaAsSb/AlGaAs strained MQWs was designed and prepared. The MQWs were rapid thermal annealed at various temperatures. Their optical properties and strain performances before and after annealing are thoroughly investigated. The LH exciton emission and the HH exciton emission are observed in all samples at room temperature. After rapid thermal annealing, the LH emission peak and HH emission peak have significant blue shift. This phenomenon can be explained in terms of the increasing of strain or interfacial diffusion. Our studies were of great significance for adjustment of optical properties in GaAsSb/AlGaAs strained MQWs.

¹State Key Laboratory of High Power Semiconductor Laser, Changchun University of Science and Technology, 7089 Wei-Xing Road, Changchun 130022, People's Republic of China. ²Department of Electrical and Electronic Engineering, Southern University of Science and Technology, Shenzhen 518055, Guangdong, People's Republic of China. ✉email: jl_tangcust@163.com; zpweicust@126.com

Sample	Annealing temperature (°C)	Rising time (s)	Keeping time (s)	Atmosphere
As grown	–	–	–	–
RTA 600	600	6	30	N ₂
RTA 700	700	6	30	N ₂
RTA 800	800	6	30	N ₂

Table 1. The parameters of rapid thermal annealing.

Methods

The strained MQWs were grown on semi-insulating GaAs (100) substrates by using DCA P600 solid source molecular beam epitaxy equipment. Before epitaxy, the substrate was transferred into MBE chamber for pre-processing to remove oxide layer at 560 °C. Subsequently, a 500 nm GaAs buffer layer was grown on substrate. The growth temperature was set to 620 °C. Then, five period of QWs consist of 15 nm GaAs_{0.92}Sb_{0.08} well layers and 25 nm Al_{0.3}Ga_{0.7}As barrier layers were grown. The growth temperature of GaAs_{0.92}Sb_{0.08} and Al_{0.3}Ga_{0.7}As was about 500 °C. All of well and barrier layers were unintentionally doped. After growth, the epitaxial wafer was split into four parts. Three parts were annealed at 600 °C, 700 °C and 800 °C, which were labeled as sample RTA 600, RTA 700 and RTA 800, respectively. The parameters of RTA were shown in Table 1.

The optical properties of GaAs_{0.92}Sb_{0.08}/Al_{0.3}Ga_{0.7}As MQWs were investigated by photoluminescence (PL) spectroscopy. A 655 nm semiconductor laser was used as excitation source. Emission signal was collected and dispersed by HORIBA iHR550 Imaging Spectrometer and detected by electric-cooled InGaAs photodetector. The spot size of laser beam was about 0.4 cm². The temperature dependent PL spectra were measured from 10 to 300 K under the excitation power of 250 mW/cm². A Janis CCS-150 closed-cycle cryogenic refrigeration system equipped with LakeShore 325 Temperature Controller was employed to control the samples temperature. All of PL spectra were measured with the temperature stability of 0.5 K. The strains of MQWs were calculated from the X-ray diffraction (XRD) spectra, which measured by using X-ray diffractometer (Bruker D8-Discover).

Results and discussion

The temperature-dependent PL spectra of all samples are shown in Fig. 1a. Emission peaks of four samples at 10 K locate at 1.407 eV, 1.410 eV, 1.413 eV and 1.427 eV, respectively. As temperature increasing from 10 to 300 K, the peak position has first blue shift and then red shift, which is attributed to the exciton fission and temperature dependent energy shrinkage⁸. The variation of emission peaks for four samples follows the same tendency. In order to reveal the emission mechanism, the relationship of peak position and temperature is analyzed. The evolution characteristics of PL peak position could be well described by Eq. (1), which is derived by O'Donnell and Chen¹⁸

$$E_g(T) = E_g(0) - S < \hbar\omega > \left(\coth \frac{< \hbar\omega >}{2kT} - 1 \right) \quad (1)$$

where $E_g(0)$ is the band gap at 0 K, S is a dimensionless coupling constant and $< \hbar\omega >$ represents an average phonon energy involved the radiative recombination process^{18,19}. The experiment results and fitting curves of temperature dependent emission peak position are shown in Fig. 1b. The solid lines are fitting curves with Eq. (1) and the discrete points are experimental results. The fitting parameters are worked out and shown in Table 2. The experimental results are well consistent with the fitting curve, which indicate that the main peak of PL spectra originate from near band emission.

Figure 2a shows the room temperature PL spectra of all samples. The main peaks of spectra locate at 1.321 eV, 1.322 eV, 1.326 eV and 1.345 eV, respectively. Notably, the shape of emission peak is asymmetry and the peak positions after annealing have a tiny blue shift compared with as grown sample. There must be more than one type of radiative recombination. Then, we employ Gaussian fitting to analyze the emission spectra and reveal the mechanism. Figure 2b shows the Gaussian fitting results of PL spectra at room temperature. The emission peak contains three parts for all samples. According to our previous work²⁰, the left two parts are related with the splitting of valence band in strained MQWs. The peak (P1) located at low energy side comes from the radiative recombination of electrons and heavy holes. The peak (P2) located at high energy side is attributed to the radiative recombination of electrons and light holes. The peak (P3) located at ~1.38 eV is attributed to the interfacial radiative recombination. Notably, the P3s in the spectra of as grown, RTA 600 and RTA 700 are so weak that can be neglected.

Then, the origins of blue shift are investigated in detail to reveal the emission mechanism of strained MQWs. The increase of compressive strain in MQWs may be the significant factor. A triple crystal XRD measurement is performed to study strain characteristics at room temperature, as shown in Fig. 3. Five satellite peaks are observed in samples as grown, RTA 600 and RTA 700, which suggested that the qualities of MQWs are perfect. But, only -1st and -2nd satellite peaks are observed in sample RTA 800. It indicates that the periodic structure of MQWs has been slightly damaged. And, more remarkable, the satellite peaks in all spectra are asymmetry. It means that the compressive strains exist in samples. As the lattice parameter of Al_{0.3}Ga_{0.7}As (5.655 Å) is similar to GaAs (5.653 Å), the strain between AlGaAs and GaAs buffer could be ignored. So, the real strain in MQWs is originated from the mismatch of AlGaAs barrier layers and GaAsSb well layers. According to X-ray diffraction theories, the real strain can be estimated by following equations²¹:

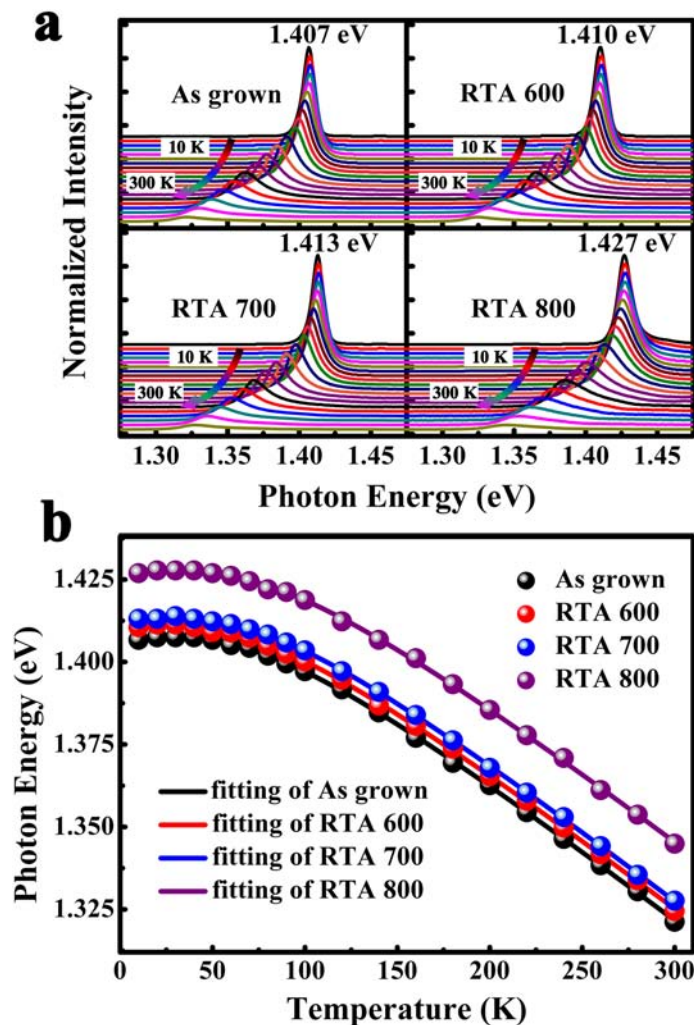


Figure 1. (a) Temperature dependent PL spectra of the GaAs_{0.92}Sb_{0.08}/Al_{0.3}Ga_{0.7}As MQWs under different annealed temperature: as grown, 600 °C, 700 °C, and 800 °C. (b) Temperature dependent emission peak positions of the MQWs samples, the solid lines are fitting curves.

Samples	As grown	RTA 600	RTA 700	RTA 800
$E_g(0)$ (eV)	1.4074 ± 0.0001	1.4108 ± 0.0001	1.4133 ± 0.0001	1.4274 ± 0.0001
S	2.56 ± 0.01	2.57 ± 0.01	2.59 ± 0.01	2.57 ± 0.02
$\langle \hbar\omega \rangle$ (meV)	21.02 ± 0.16	21.45 ± 0.15	21.52 ± 0.14	23.14 ± 0.27

Table 2. The fitting results of parameters in Eq. (1).

$$\varepsilon = \text{ctg}\theta_e \cdot \Delta\theta \quad (2)$$

$$\Delta\theta = \theta_e - \theta_s \quad (3)$$

where θ_e is the Bragg angle of GaAsSb, θ_s is the Bragg angle of AlGaAs, $\Delta\theta$ presents the shift of zero-order peak and ε is the real strain between AlGaAs and GaAsSb²⁰. The $\Delta\theta$ values for four samples are 0.010°, 0.011°, 0.013° and 0.008°, respectively. Then, the ε values of all samples were calculated to be -2.684×10^{-4} , -2.952×10^{-4} , -3.489×10^{-4} and -2.147×10^{-4} , respectively, by using the Eqs. (2)–(3). The minus sign present compressive strain. we work out that.

An elastic continuum theory is employed to investigate the band splitting under strain. The effective band gap of heavy holes and light holes in GaAsSb under strain could be calculated by following equations^{22,23}.

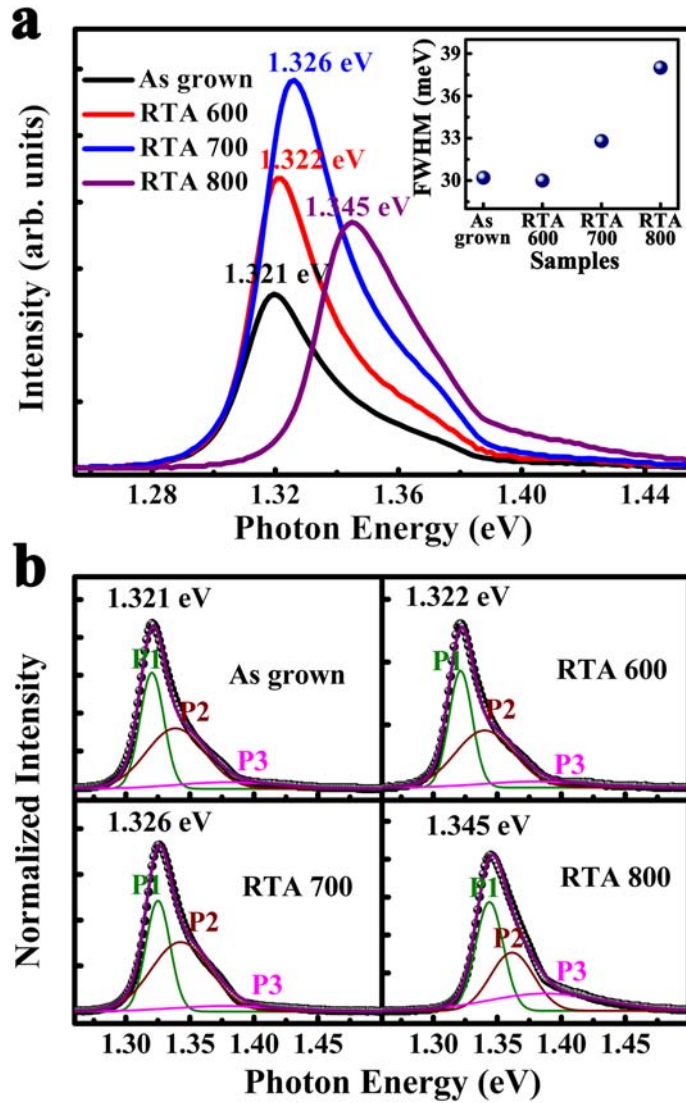


Figure 2. (a) The room temperature PL spectra of all MQWs samples. The insert is FWHM of PL spectra. (b) The Gaussian fitting results of all room temperature PL spectra for all samples.

$$E_{c-HH} = E_g^{QW}(x) + 2a \left(1 - \frac{C_{12}}{C_{11}}\right) \varepsilon - b \left(1 + 2 \frac{C_{12}}{C_{11}}\right) \varepsilon \tag{4}$$

$$E_{c-LH} = E_g^{QW}(x) + 2a \left(1 - \frac{C_{12}}{C_{11}}\right) \varepsilon + b \left(1 + 2 \frac{C_{12}}{C_{11}}\right) \varepsilon \tag{5}$$

$$a = a_c - a_v \tag{6}$$

where $E_g^{QW}(x)$ is the band gap of $\text{GaAs}_{1-x}\text{Sb}_x$ well layer without strain, a_c and a_v are the conduction band and valence band deformation potential, b is the shear deformation potential, C_{11} and C_{12} are elasticity modulus. The parameters values of GaAs, GaSb and AlAs are shown in Table 3²².

The band gap of $\text{GaAs}_{1-x}\text{Sb}_x$ bulk without strain can be estimated by Vegard's law²⁴:

$$E_g^{3D}(x) = 1.43 - 1.9x + 1.2x^2 \tag{7}$$

When the thickness of well layer reduced to the Bohr radius of excitons, the quantum confinement effect will lead to broadening of band gap. The band gap of well layer material can be estimated by following equation²⁵:

$$E_g^{QW} = E_g^{3D} + \left[\frac{\hbar^2 \pi^2}{2m_e d_w^2} + \frac{\hbar^2 \pi^2}{2m_h d_w^2} \right] \tag{8}$$

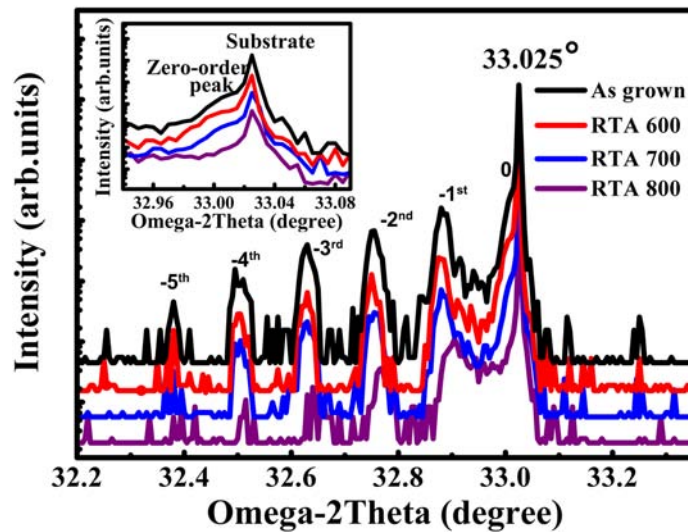


Figure 3. Triple-crystal X-ray diffraction patterns of all MQWs samples. The insert is partial enlarged XRD spectra from 32.95° to 33.08°.

	a (Å)	C_{11} (10^{11} dyn cm^{-2})	C_{12} (10^{11} dyn cm^{-2})	a_c (eV)	a_v (eV)	b (eV)
GaAs	5.6532	11.9	5.38	- 6.3 ~ - 18.3	- 0.06 ~ - 2.1	- 1.16 ~ - 2.1
GaSb	6.0959	8.834	4.023	- 7.5	- 0.8	- 1.8 ~ - 2.0
ALAs	5.6611	-	-	-	-	-

Table 3. The material parameters of GaAs, GaSb and ALAs.

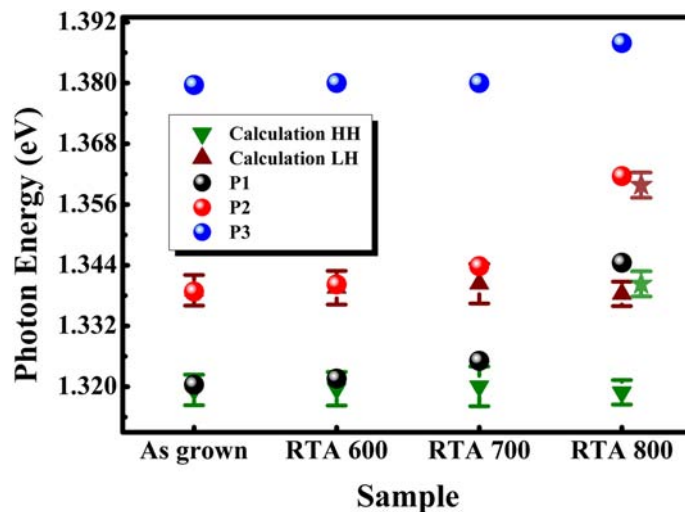


Figure 4. The evolution of P1, P2, P3 and the calculation results of HH and LH emission for different samples. The star symbols are calculation results for GaAs_{0.932}Sb_{0.068}.

where E_g^{QW} is the band gap of well layer under quantum size effect. m_e and m_h are the electron effective mass and hole effective mass. d_w is width of well layer²⁵. Based on the Eqs. (2)–(8), the effective band gaps of GaAs_{0.92}Sb_{0.08} heavy and light holes exciton in the MQWs at 300 K are calculated out and the results are shown in Fig. 4. The results calculated from elastic continuum theory are identity with experimental results for samples of as grown and RTA 600. It means that the increase of strain is main factor for blue shift under the condition of low temperature RTA.

However, the calculation results for RTA 700 and RTA 800 are smaller than experimental results. And the difference between theory and experimental results gradually increases with annealing temperature increasing. Especially for RTA 800, although its strain is smaller than that of RTA 700, the emission peaks have blue shift in experiment results. Therefore, there must be other factors affecting the emission properties.

The interfacial diffusion, which existed in semiconductor heterojunction interface, may be the other significant factor for the blue shift of emission peak in sample of RTA 800. It has been confirmed by the broken of periodicity structure of MQWs from XRD spectra. Owing to the concentration gradient between well layers and barrier layers, Sb atom migrates from GaAsSb to AlGaAs, which leads to the decrease of Sb component in well layer^{26,27}. So, the band gap of GaAsSb is broadened and the height of valence-band offsets is reduced. In this case, the interface related emission is enhanced and the peak position has blue shift (Fig. 4). Furthermore, when the annealing temperature increase up to 800 °C, the degeneration of interface caused by interfacial diffusion will greatly increase interfacial radiative recombination, which is consistent with the PL spectra in Fig. 2b. In addition, as the interfacial emission of quantum well increasing, the full width of half maximum (FWHM) of PL spectra will greatly broaden (Insert of Fig. 2a).

As is known to all, the diffusion rate depends on annealing temperature. Meanwhile, it can be also enhanced by the compressive strain in MQWs and vacancy concentration. The diffusion coefficient related to temperature is according to Arrhenius equation²⁸:

$$D = D_0 e^{\left(\frac{-Q_d}{RT}\right)} \quad (9)$$

where D_0 is the temperature-independent preexponential, Q_d is the activation energy. As can be seen from the equation, the diffusion coefficients increase with increasing of annealing temperature. Under conditions of nonsteady state, Fick's second law is used to calculate the distribution of concentration. The Sb component is estimated to be about 0.068 in GaAs_{1-x}Sb_x of sample RTA 800. And then, the Sb component is substituted into the Eqs. (4)–(8) to calculate the HH and LH emission peaks. The calculation values are also shown in Fig. 4 (star symbol), which is consistent with experimental data. Considering the above analyses, we conclude that the interfacial diffusion is the main significant factor for the blue shift of emission peak of RTA 800.

Conclusions

In summary, the effect of rapid thermal annealing on strained GaAs_{0.92}Sb_{0.08}/Al_{0.3}Ga_{0.7}As MQWs is analyzed in detail. The crystal quality and strain properties of samples are analyzed by using XRD. The elastic continuum theory is employed to calculate the strain and the band gap of strained MQWs. After annealing, the light holes exciton emission and heavy holes exciton emission have blue shift. At low annealing temperature, the blue shift is attributed to the increase of interfacial strain. But, when annealing temperature is higher than 800 °C, the blue shift is mainly due to the interfacial diffusion between barrier layers and well layers. Our work presents a detailed study on the emission characteristics variation of strained MQWs caused by rapid thermal annealing, which is significance for enhancing the performance of GaAsSb based MQWs laser.

Received: 28 October 2020; Accepted: 28 December 2020

Published online: 12 January 2021

References

- Liu, J. S., Clavel, M. & Hudait, M. K. Tailoring the valence band offset of Al₂O₃ on epitaxial GaAs_{1-y}Sb_y with tunable antimony composition. *ACS Appl. Mater. Inter.* **7**, 28624–28631 (2015).
- Motyka, M. *et al.* Type-II quantum wells with tensile-strained GaAsSb layers for interband cascade lasers with tailored valence band mixing. *Appl. Phys. Lett.* **108**, 101905 (2016).
- Teissier, R. *et al.* Temperature-dependent valence band offset and band-gap energies of pseudomorphic GaAsSb on GaAs. *J. Appl. Phys.* **89**, 5473–5477 (2001).
- Zhu, H., Liu, K., Xiong, C., Fen, S. & Guo, C. The effect of external stress on the properties of AlGaAs/GaAs single quantum well laser diodes. *Microelectron. Reliab.* **55**, 62–65 (2015).
- Balgos, M. H. *et al.* Temperature behavior of unstrained (GaAs/AlGaAs) and strained (InGaAs/GaAs) quantum well bandgaps. *Opt. Quant. Electron.* **47**, 3053–3063 (2015).
- Dong, H. *et al.* Influence of substrate misorientation on the photoluminescence and structural properties of InGaAs/GaAsP multiple quantum wells. *Nanoscale* **8**, 6043–6056 (2016).
- Chiu, Y. S., Ya, M. H., Su, W. S. & Chen, Y. F. Properties of photoluminescence in type-II GaAsSb/GaAs multiple quantum wells. *J. Appl. Phys.* **92**, 5810–5813 (2002).
- Gao, X. *et al.* Investigation of localized states in GaAsSb epilayers grown by molecular beam epitaxy. *Sci. Rep.* **6**, 29112 (2016).
- Fang, X. *et al.* Influence of exciton localization on the emission and ultraviolet photoresponse of ZnO/ZnS core-shell nanowires. *ACS Appl. Mater. Inter.* **7**, 10331–10336 (2015).
- Zhu, Y. *et al.* Defect assistant band alignment transition from staggered to broken gap in mixed As/Sb tunnel field effect transistor heterostructure. *J. Appl. Phys.* **112**, 094312 (2012).
- Liao, Y. A., Hsu, W. T., Chiu, P. C., Chyi, J. I. & Chang, W. H. Effects of thermal annealing on the emission properties of type-II InAs/GaAsSb quantum dots. *Appl. Phys. Lett.* **94**, 053101 (2009).
- Bian, L. F., Jiang, D. S. & Lu, S. L. Optical investigation on the annealing effect and its mechanism of GaInAs/GaNAs quantum wells. *J. Cryst. Growth* **253**, 155–160 (2003).
- Khreis, O. M. Interdiffusion and the strain effect in pseudomorphic quantum well heterostructures. *Solid State Commun.* **132**, 767–771 (2004).
- Govindaraju, S., Reifsnider, J. M., Oye, M. M. & Holmes, A. L. Time and temperature dependence on rapid thermal annealing of molecular beam epitaxy grown Ga_{0.8}In_{0.2}N_{0.01}As_{0.99} quantum wells analyzed using photoluminescence. *Jr. J. Electron. Mater.* **32**, 29–33 (2003).
- Karimi, M. J. Intense laser field effects on the electron Raman scattering in a strained InGaN/GaN quantum well. *Phys. E* **66**, 18–23 (2015).

16. Cesar, D. F. *et al.* Contrasting LH-HH subband splitting of strained quantum wells grown along [001] and [113] directions. *Phys. Rev. B* **81**, 233301 (2010).
17. Zhuang, Q. D. *et al.* Effect of rapid thermal annealing on InGaAs/GaAs quantum wells. *J. Cryst. Growth* **212**, 352–355 (2000).
18. O'Donnell, K. P. & Chen, X. Temperature dependence of semiconductor band gaps. *Appl. Phys. Lett.* **58**, 2924–2926 (1991).
19. Wang, D. K. *et al.* Optical properties improvement of GaSb epilayers through defects compensation via doping. *J. Lumine* **197**, 266–269 (2018).
20. Gao, X. *et al.* The strain, energy band and photoluminescence of GaAs_{0.92}Sb_{0.08}/Al_{0.3}Ga_{0.7}As multiple quantum wells grown on GaAs substrate. *Solid State Commun.* **309**, 113837 (2020).
21. Bennett, B. R., Chick, T. F., Boos, J. B., Champlain, J. G. & Podpirka, A. A. Strained InGaAs/InAlAs quantum wells for complementary III–V transistors. *J. Cryst. Growth* **388**, 92–97 (2014).
22. Vurgaftman, I., Meyer, J. R. & Ram-Mohan, L. R. Band parameters for III-V compound semiconductors and their alloys. *J. Appl. Phys.* **89**, 5815–5875 (2001).
23. Wang, T. S. *et al.* Characterization of band gap in GaAsSb/GaAs heterojunction and band alignment in GaAsSb/GaAs multiple quantum wells. *Mater. Sci. Eng. B Adv.* **147**, 131–135 (2008).
24. Liu, G., Chuang, S. L. & Park, S. H. Optical gain of strained GaAsSb/GaAs quantum-well lasers: a self-consistent approach. *J. Appl. Phys.* **88**, 5554–5561 (2000).
25. Brus, L. E. Electron-electron and electron-hole interactions in small semiconductor crystallites: the size dependence of the lowest excited electronic state. *J. Chem. Phys.* **80**, 4403–4409 (1984).
26. Gillin, W. P., Sealy, B. J. & Homewood, K. P. Thermal interdiffusion in InGaAs/GaAs and GaAsSb/GaAs strained quantum wells as a function of doping density. *Opt. Quant. Electron.* **23**, S975–S980 (1991).
27. Dang, Y. X. *et al.* Interdiffusion effect on GaAsSbN/GaAs quantum well structure studied by 10-band k.p model. *Thin Solid Films* **515**, 4435–4440 (2007).
28. Kube, R. *et al.* Composition dependence of Si and Ge diffusion in relaxed Si_{1-x}Ge_x alloys. *J. Appl. Phys.* **107**, 073520 (2010).

Acknowledgements

This work is supported by the National Natural Science Foundation of China (Nos. 61574022, 61674021, 11674038, 61704011, 61904017), the Developing Project of Science and Technology of Jilin Province (Nos. 20160520027JH, 20170520117JH), the Youth Foundation of Changchun University of Science and Technology (No. XQNJJ-2018-18), the China Postdoctoral Science Foundation (No. 2019M652176) and Shenzhen Fundamental Research Program (No. JCYJ20180307151538972).

Author contributions

D.K.W., R.C. and Z.P.W. wrote the main manuscript text, D.F. and X.F. prepared Figures, X.G. and J.L.T. performed epitaxy of quantum wells, X.W.W. and F.Y.L. performed XRD and X.H.W. performed photoluminescence spectra. All authors reviewed the manuscript.

Competing interests

The authors declare no competing interests.

Additional information

Correspondence and requests for materials should be addressed to J.T. or Z.W.

Reprints and permissions information is available at www.nature.com/reprints.

Publisher's note Springer Nature remains neutral with regard to jurisdictional claims in published maps and institutional affiliations.



Open Access This article is licensed under a Creative Commons Attribution 4.0 International License, which permits use, sharing, adaptation, distribution and reproduction in any medium or format, as long as you give appropriate credit to the original author(s) and the source, provide a link to the Creative Commons licence, and indicate if changes were made. The images or other third party material in this article are included in the article's Creative Commons licence, unless indicated otherwise in a credit line to the material. If material is not included in the article's Creative Commons licence and your intended use is not permitted by statutory regulation or exceeds the permitted use, you will need to obtain permission directly from the copyright holder. To view a copy of this licence, visit <http://creativecommons.org/licenses/by/4.0/>.

© The Author(s) 2021